Hydro-structural behaviour of LNG membrane containment systems under breaking wave impacts: findings from the Sloshel project

H. Bogaert[1,2], *S. Léonard*[3], *M. Marhem*[3], *G. Leclère*[3], *and M. Kaminski*[1]

[1]*Hydro Structural Services, MARIN, Wageningen, the Netherlands*
[2]*Delft University of Technology, Ship Structures Laboratory, Delft, Netherlands*
[3]*Technical dept, GTT (Gaztransport & Technigaz), Saint-Rémy-lès-Chevreuse, France*

ABSTRACT

The behaviour of the NO96 membrane containment system when subjected to breaking waves is presented in this paper. The data obtained from the full scale impact tests in the Sloshel project are used. Uni-directional breaking waves were generated and interacted with a real membrane containment system.

Three types of hydro-structural interaction can be distinguished based on the relative position between load durations and natural periods. The aim of this paper is to identify which type of interaction occurred between the breaking wave and the NO96. It is demonstrated that it is not straightforward to define the interaction type by a comparison of observed load durations and predefined mode shapes. As an alternative, it was investigated whether the type of interaction can be deduced from its effect on the load and on the response with respect to a quasi-static interaction.

KEY WORDS

Hydro-structural interaction, membrane containment systems, sloshing, wave impact.

INTRODUCTION

The use of numerical simulations to assess membrane containment systems subjected to sloshing is beyond the state-of-the-art. The only tool available today for such an assessment is model tests at small scale. However, the tests represent an experimental modeling of the reality. One of the difficulties is that the response of the containment system is not directly obtained, because the tank walls are rigid in the model tests.

The structural response needs therefore to be calculated based on the measured loads, taking the mutual interaction between load and response into account. The difficulty here lies in the fact that a large database of measured pressures needs to be processed. It is time-consuming to perform a structural analysis for each sloshing event. Furthermore, it is not straightforward to include the hydro-structural interaction after the interaction took place.

Dynamic amplification factors are used today in combination with a statistical treatment of the measured pressures as an engineering approach to include the dynamic effect of the load on the structural response. The influence of the structural response on the load is thereby not taken into account.

The data obtained from the full scale impact tests in the Sloshel project is used to examine the validity of this engineering approach. In this paper, we focus on the question to which extent (1) dynamic effects of the load on the response and (2) influences of the response on the load, occur during a wave impact on a membrane system at ambient temperatures.

The paper is organised as followed: first, the test set-up of the Sloshel full scale tests is briefly described. Three types of hydro-structural interactions are discussed next. They are a function of the relative position between load durations and natural periods. After which, observations of the interaction between load and response are presented. Slosh and air pocket impacts are illustrated. An evaluation is made of the observed load durations in order to define the types of hydro-structural interaction that occured during full scale testing. In addition, it was investigated whether the type of interaction can be deduced from its effect on the load and on the response with respect to a quasi-static interaction. Therefore, a stiffness matrix based on the experiments was determined and the effect of local loads was studied.

IMPACT TESTS

The test method and the experimental setup of the Sloshel full scale tests are described in Kaminski and Bogaert (2010). The tests were especially designed to study the hydro-structural interaction (Figure 1). In each test, uni-directional breaking waves

interacted with a rigid concrete structure and a NO96 containment system simultaneously. Standard reinforced NO96 boxes were tested. Pressure sensors were installed to measure the load on both structures. Strain gauges and accelerometers were used to measure the response of the NO96 box.

(a) (b) (c) (d)

FIGURE 1: Full scale test - rigid structure at the left (grey) and NO96 box at the right (yellow).

The position of the pressure and the strain gauges on the NO96 primary box are given in Figure 2. Sensor labels that are introduced, will be used throughout this paper. On the cover plate of the NO96, strain gauges and accelerometers are installed at the same locations as the pressure sensors, with exception of P14 and P17. The strain gauges are mounted on the inner surface of the cover plate and are oriented perpendicularly to the bulkheads, indicating the bending of the cover plate between two bulkheads. The compression and the bending strain of the primary and secondary bulkheads were also measured. The focus in this paper is on the primary box. Four strain gauges were installed at each side of the primary bulkheads. The double bulkheads 3 and 7 were not instrumented.

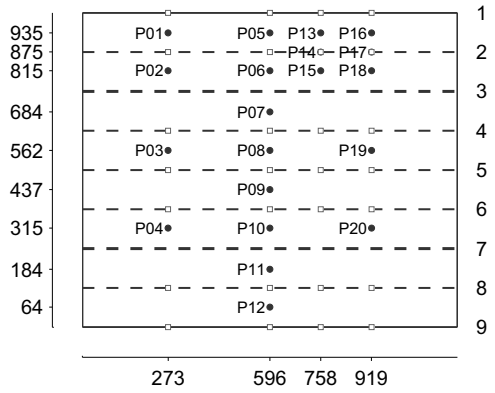

FIGURE 2: Position of pressure and strain gauges on NO96 primary box - (○) indicates sensors on cover plate and (□) on bulkheads.

THREE TYPES OF HYDRO-STRUCTURAL INTERACTION

The interaction that occurred between the wave and the NO96 box is in theory governed by at least two time scales, namely one related to the load duration T_L and another related to the response duration. The time scale related to the response of the structure is in the order of its natural period T_S. The relative position of these durations define three regions of hydro-structural interaction:

1. $T_L \ll T_S$, two stages can be identified with a time scale of respectively T_L and T_S. In the first stage, the wave impacts the structure. The hydrodynamic load accelerates the structure. Since T_L is small, integrating this acceleration twice in time implies that the deformation of the structure - in contrast to its acceleration and velocity - is still negligible in the first stage. The inertia accordingly counterbalances the hydrodynamic load. Moreover, part of the hydrodynamic load is proportional to the acceleration of the structure and results by integration in the so-called hydrodynamic mass.

   In the second stage, the wave gradually loads the structure while it interacts with the free vibration of the structure, induced at the first stage. The hydrodynamic mass becomes predominant in the hydrodynamic pressure. At the end, the pressure oscillations and structural vibrations die down because of damping.

2. $T_L \approx T_S$, the hydrodynamic load accelerates the structure during a time scale identical to the natural period of the structure. Therefore, integrating the acceleration twice in time implies that the inertia forces - including the hydrodynamic mass - and the elastic forces mainly counterbalance each other. As a consequence, the remainder of the hydrodynamic load mainly needs to overcome the damping force.

3. $T_L \gg T_S$, the hydrodynamic load acts slowly relative to the natural period of the structure and therefore hardly accelerates the structure. Since T_L is large, integrating this acceleration twice in time, implies that the deformation will be significantly compared to the acceleration and the velocity. The elastic force accordingly counterbalances the applied load. The hydrodynamic mass will be small and the fluid dynamics are hardly influenced by the structure.

The difficulty of defining which type of interaction occurred during the full scale tests, is to understand which load duration T_L is related to which structural mode T_S. Different load characteristics might occur during the impact of a breaking wave. This is illustrated next.

OBSERVATIONS

The full scale tests were classified into four impact types, i.e aerated, air pocket, flip-through and slosh, depending on the advancement of the breaking process (see Kaminski and Bogaert (2010)). Air pocket and slosh impacts are used in this paper to illustrate the hydro-structural interaction.

Slosh impact

The wave does not break before the wall in case of a slosh impact. When the wave approaches the wall, the wave trough runs up along the wall and reaches the anticipated impact zone way

before the wave crest, resulting in small pressures with long durations. The load successively builds up along the wall, apparent in terms of a time delay in the pressure profile. The pressure starts to build up when the trough passes by. The velocity of the trough defines the pressure profile. Two slosh impacts are given in Figure 4 with a different trough velocity.

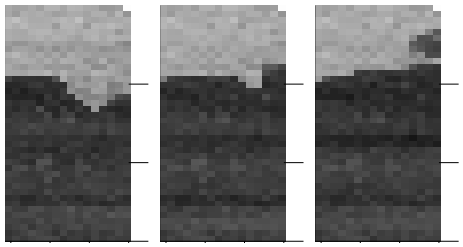

(a) (b) (c)

FIGURE 3: Slosh impact. Pressure profile given in Figure 4a.

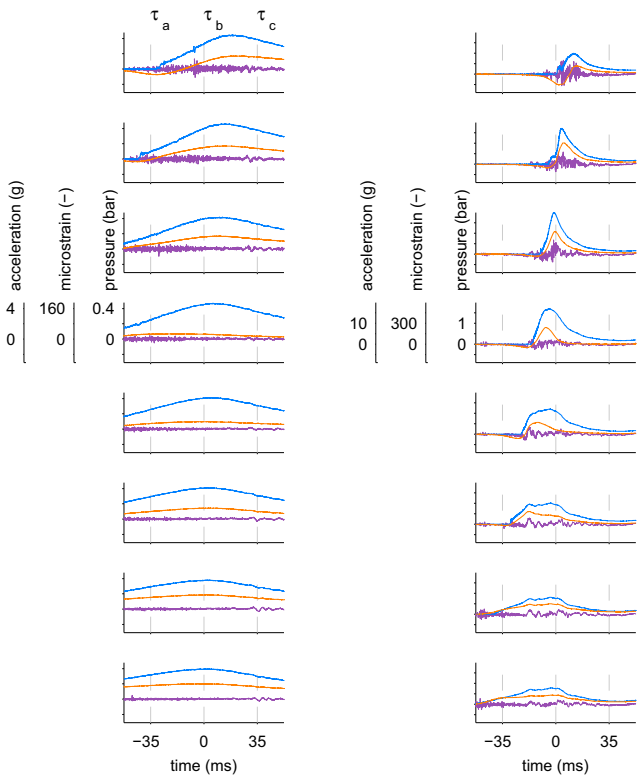

(a) (b)

FIGURE 4: Pressure (—), strain (—) and acceleration (—) on cover plate of NO96 for slosh impact. Wave shape at time instant τ_i given in Figure 3 for (a). Pressure sensor P05 to P12 are shown.

It is apparent from Figure 4 that for a slosh impact the interaction between the load and the response is quasi-static. The accelerations are small and the elastic force counterbalances the load.

The response of the cover plate shows a similar pattern as the load. However, local differences can be observed because deformation modes other than the bending of a cell are also involved. Here, a cell is defined as the part of the cover plate between two bulkheads. The measured deformation can be considered as a combination of different structural modes, whereby one or more are predominant. The fact that structural deformation is present before a cell is loaded (see Figure 4), indicates that modes - spatially more global than the bending of a cell - are involved. The cell deflects upwards when the trough loads the cell underneath.

The presence of global modes can furthermore be deduced from the response of the primary bulkheads. The vertical strain on the middle of the bulkheads are shown in Figure 5 for the slosh impacts considered in Figure 4. The strain is measured at both sides of the bulkheads and decomposed in a component due to bending and due to axial loading. The response in the bulkheads builds up along the box with the delay as observed for the load. However, the strain on the bulkheads is not equal. This indicates that modes, spatially more global than the bending of a cell, play a roll.

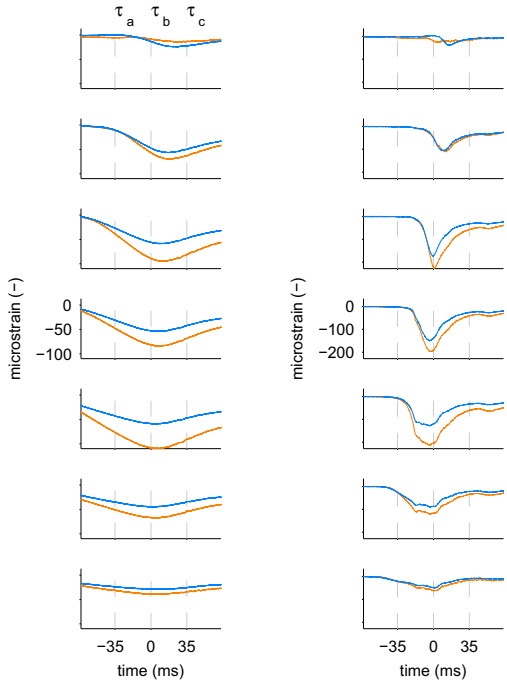

(a) (b)

FIGURE 5: Strain at the middle of primary bulkheads for slosh impact of Figure 4. Strain due to bending (—, top side of bulkhead) and due to axial loading (—).

Finally, local differences between the load and the response can also result from three-dimensional structural aspects. It is observed that a two-dimensional load does not result in a two-dimensional response. Illustrations are given in Figure 6 for the slosh impacts considered in Figure 4. The load on and the response of a cell is given in combination with its adjacent bulk-

head. The response near the middle of the box will differ from those near the boundaries since the box has a finite size. However, this explains only partially the three-dimensional response. Staples, used for the assembly of the boxes, can introduce this local behaviour. This is studied later on in this paper.

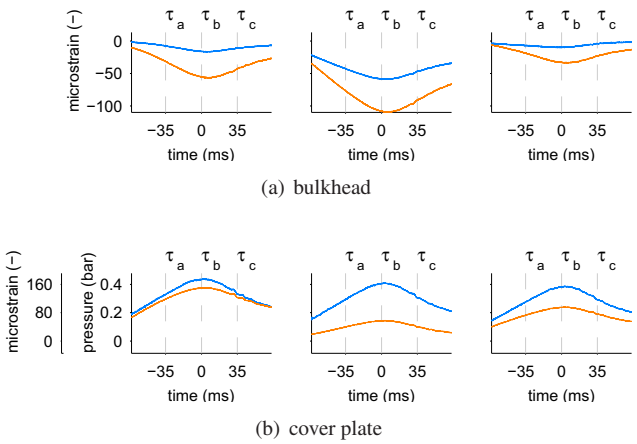

FIGURE 6: Slosh impact considered in Figure 4a - (a) vertical strain on bulkhead 6. Strain due to bending (—, top side of bulkhead) and due to axial loading (—). (b) pressure (—) and strain (—) on cover plate. Pressure sensor P04, P10 and P20 are shown.

Air pocket impact

When the wave breaks before the wall, an air pocket is entrapped. Two pressure distributions are present, i.e. high pressures with short duration due to the impinging wave crest and low pressures with long duration acting on a large area due to the compression of the air pocket. At the moment the pocket closes, the air is compressed and the pressure within the pocket starts to build up. The air volume is successively compressed and expanded during impact, resulting in pressure oscillations. The smaller the volume of the entrapped air, the higher the frequency of oscillation. Two air pocket impacts are given in Figure 8 with a different location of the crest. Further, the air pocket is smaller in case of Figure 8a.

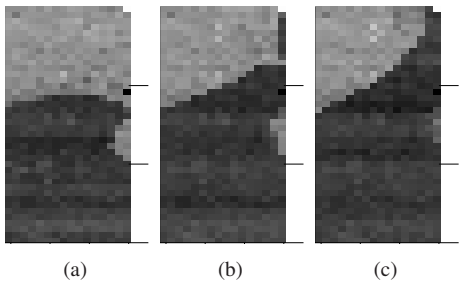

FIGURE 7: Air pocket impact. Pressure profile given in Figure 8a.

The interaction between the air pocket itself and the NO96 is quasi-static. The accelerations are small within this region. The

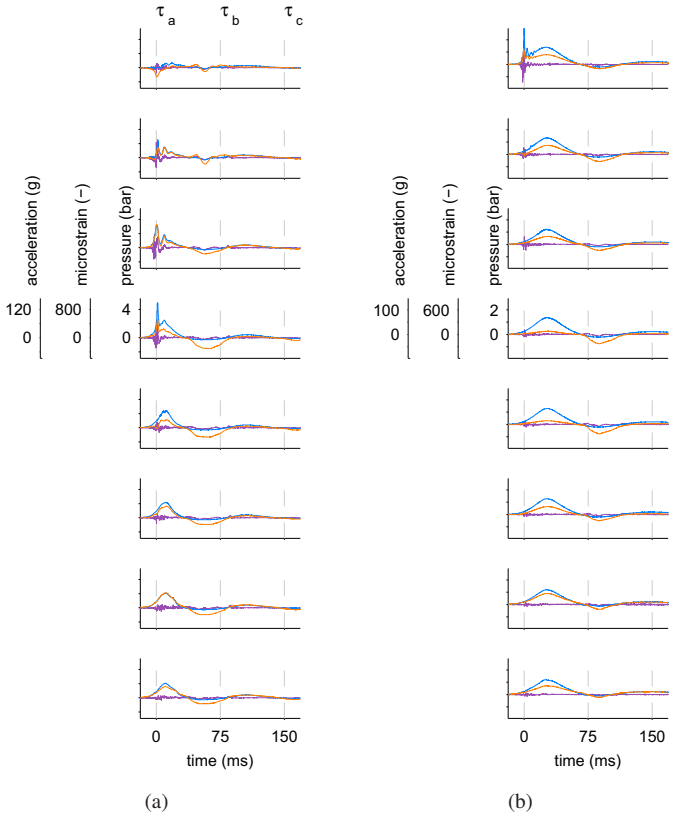

FIGURE 8: Pressure (—), strain (—) and acceleration (—) on cover plate of NO96 for air pocket impact. Wave shape at time instant τ_i given in Figure 7 for (a). Pressure sensor P05 to P12 are shown.

elastic force counterbalances the load, characterized by the frequency of the air pocket oscillation. The oscillation present in the response of the cover plate should therefore not be confused with a free vibration of the cover plate after excitation. This can be deduced from the fact that no significant acceleration with this frequency is present.

During the compression of the air pocket, the primary bulkheads are bent and axially loaded (see Figure 9). During the expansion of the air pocket, on the other hand the bulkheads deform little while the cover plate deflects relatively more. The gas pocket pressure is below the atmospheric pressure during expansion. Furthermore, the amplitude of the pressure during compression and expansion are not equal at full scale. This is explained in Bogaert et al. (2010). During expansion, the pressure inside the box is thus higher than the pressures at the contact surface. The cover plate therefore deflects outwards. The bulkheads - stapled to the cover plate - are lightly loaded. This can be mainly observed in the middle vertical line of the box. Figure 10 shows the fourth primary bulkhead for the air pocket impact considered in Figure 8b. Different staple connections are apparent. During expansion, the bulkhead is lightly compressed on the left side, unloaded in the middle and under tension on the right side. It can be concluded that (1) the deformation mode changes during impact and (2) a

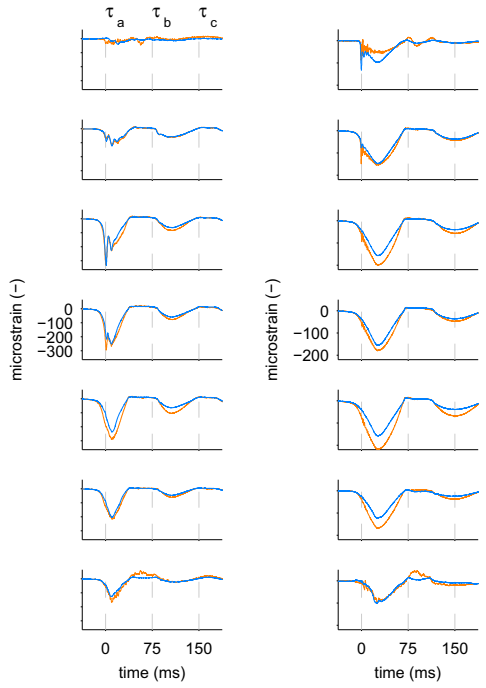

FIGURE 9: Strain at the middle of primary bulkheads for air pocket impact of Figure 8. Strain due to bending (—, top side of bulkhead) and due to axial loading (—).

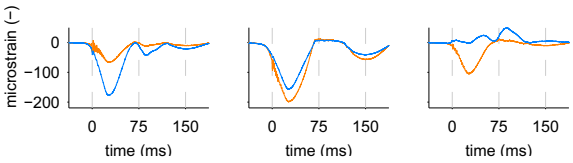

FIGURE 10: Air pocket impact considered in Figure 8b - Vertical strain on fourth primary bulkhead. Strain due to bending (—, top side of bulkhead) and due to axial loading (—).

two-dimensional load within the air pocket does not result in a two-dimensional response as a result of different staple connections.

After the first expansion, the box is compressed again in a quasi-static way. However, for some air pocket impacts, vibrations of the box were measured after the first expansion. This was observed when the wave trough and crest focus together at the upper side of the box and entrap a smalls air pocket. Higher velocities of the trough are involved. The load and response of the NO96 are shown in Figure 11. The main component in the hydrodynamic load after expansion is the hydrodynamic mass induced by the free vibration. The hypothesis is: when the spring washer in the couplers is compressed maximally during the expansion of the air pocket, the box is pushed back towards the wall, resulting in an excitation of the assembly. The couplers are used to anchor the primary and secondary box to the ship structure. The coupler is fixed to the inner hull through a ball-joint. Spring washers make the coupler elastic. A schematic representation is given in Figure 12.

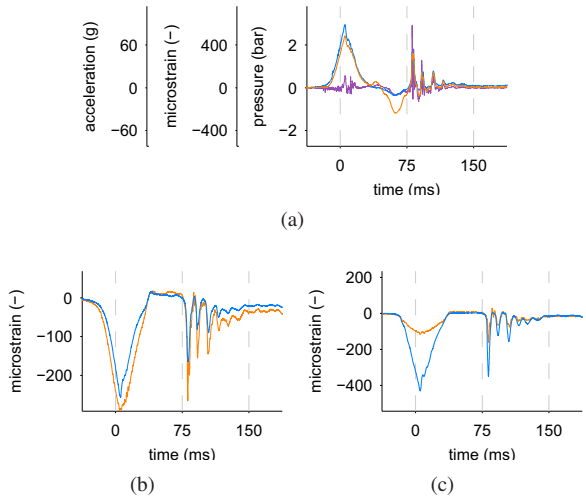

FIGURE 11: Vibration after expansion of air pocket. (a) pressure (—), strain (—) and acceleration (—) on cover plate. (b) and (c) vertical strain on primary and secondary bulkheads respectively. Strain due to bending (—) and due to axial loading (—). Pressure sensor P10 is shown. Strain given at middle of primary bulkhead and nearest location on secondary bulkhead.

FIGURE 12: Schematic representation of couplers used to anchor the NO96 to the inner hull

As shown in Figure 13, the load within the crest is not two-dimensional. The high speed video recordings in Figure 14 illustrate how fragmented the crest is during impact. The recordings are obtained from the large scale tests (see Bogaert and Kaminski (2010)). After hitting the wall, the crest is forced to adapt its shape in order to avoid the structure, resulting in a vertical jet. This rapid change of momentum results in high pressures. However, the highest pressures will be measured at the initial contact point between the crest and the structure. This initial contact point is very localised because (1) the front of the crest is not vertical owing to the fact that air is escaping between crest and structure before impact and (2) the crest is not two-dimensional. In gen-

eral, the crest load will therefore be captured only partially by a discrete set of pressure gauges.

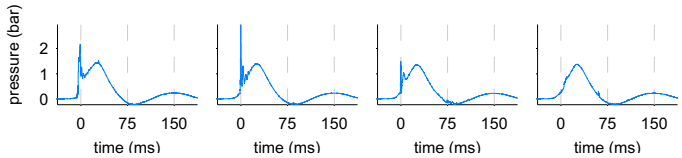

FIGURE 13: Pressure on cover plate of NO96 for air pocket impact considered in Figure 8b. Pressure sensor P01, P05, P13 and P16 are shown.

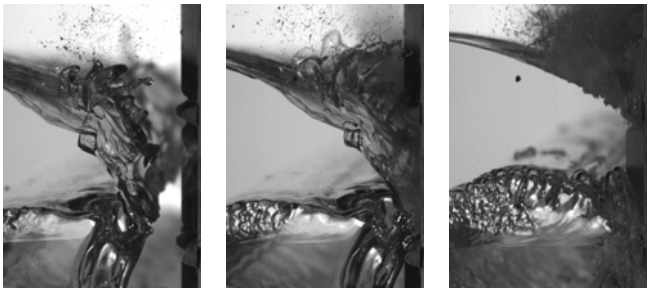

(a) (b) (c)

FIGURE 14: Wave crest during impact

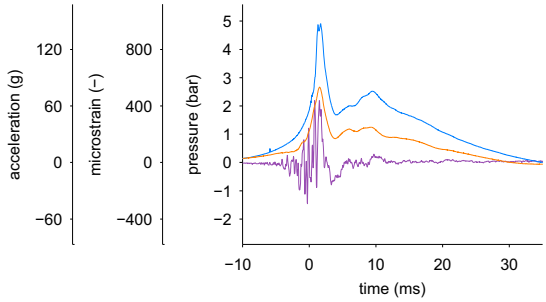

(a)

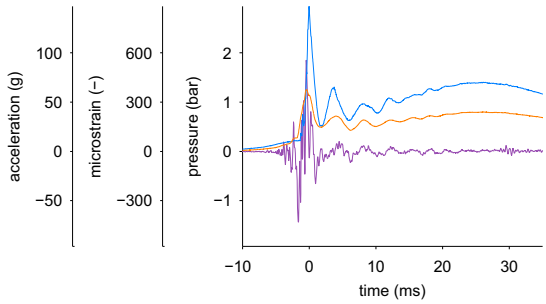

(b)

FIGURE 15: Air pocket impact Figure 8a and b - pressure (—), strain (—) and acceleration (—) on cover plate.

The measured pressure at the crest consists of three parts: (1) a pressure peak followed by (2) high frequency oscillations combined with (3) pressure oscillations related to the compression of the air pocket. Details of the pressure in the crest are given in Figure 15 for the air pocket impacts of Figure 8. The response in the cover plate and bulkheads show locally the same pattern, see Figure 15 and 9. However, the interaction between the crest and the NO96 is not quasi-static. High accelerations are observed during the pressure peak. At this time instant, accelerations can also be observed at the region above the crest and within the air pocket. The accelerations are smaller when located further away from the crest. The effect of the crest is therefore not only local.

After the pressure peak, the accelerations are in phase with the high frequency oscillations in the strain and the hydrodynamic load. This component of the load is the added mass due to the free vibration of the structure, excited by the pressure peak. This vibration is combined with the air pocket oscillation. It is apparent that a different vibration occurs in case of Figure 8a and b. In addition, Figure 8a shows that the vibrations are mainly present above the location of the pressure peak. At the end, the high frequency oscillations die down and the interaction becomes quasi-static. The accelerations are small and the elastic force counterbalance the air pocket load.

NATURAL PERIODS AND LOAD DURATIONS

From the observations, it can be concluded that the higher the loads are, the smaller the loaded area and the shorter the load durations will be. For global loads such as the trough loading or the air pocket loading, a quasi-static interaction occurred. For local loads such as the crest loading, the interaction appeared not to be quasi-static, because high accelerations are present. However, it is not yet clear whether the load duration T_L is smaller than or equal to the natural period of the structure T_S.

A numerical example is studied first. The outer cell of the NO96 is impacted by a sinusoidal load. The load duration is in the order of the first natural mode shape of the cell (T=0.5ms). The sinus shape is chosen to avoid high frequency content. The displacement of the cover plate is given at successive time instants in Figure 16. The primary bulkheads and the secondary box are not visualised. First, the load accelerates the cell during a time scale identical to the natural period of the cell. After that, the cover plate starts to vibrate with a period around 2ms. At the cell, the deformation becomes a combination of these modes.

In this example, the load is in the order of the natural period of the cell ($T_L \approx T_{S_{cell}}$) and shorter than the natural period of the cover plate ($T_L \ll T_{S_{cover}}$). If the interaction type was studied based on the natural period of the cover plate, the conclusion would be that the local load is filtered by the structure. However, the local load first interacts with more local modes that have shorter natural periods. Three options are possible: (1) the local load has a load duration that is shorter than the natural period related to this area, (2) the local load has a load duration that is in the same order of the natural period related to this area or (3) the local load has a load duration that is longer than the natural period related to this

area. Global modes are involved afterwards and do therefore not necessarily affect the peak pressure.

It can be concluded that peak loads are not necessarily filtered completely by the structure, as has been observed in Figure 15, just because they are related to small loaded areas and short load durations. It was furthermore observed that the global modes following the peak pressure differ when the crest strikes the NO96 at a different location. Evaluation of the structural response for a pressure peak depends on the loading of the whole NO96 even though it is partially quasi-static.

It remains however not straightforward to conclude on the type of interaction for the local crest loading, because the loaded area is inevitably not well defined and therefore as well the natural period related to it. An alternative to this comparison between load durations and natural periods, is studied next.

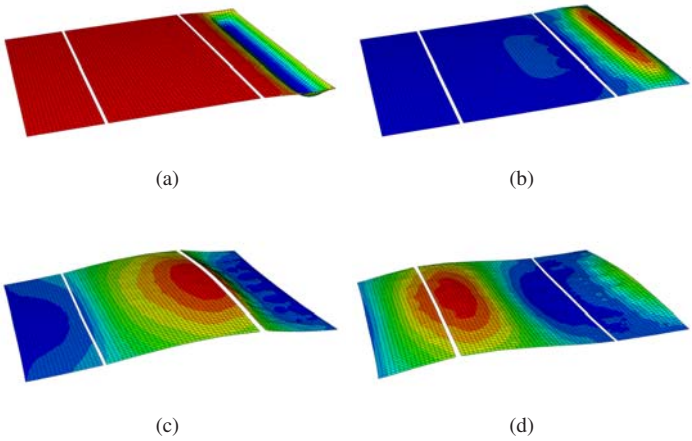

FIGURE 16: Structural deformation during loading of upper NO96 cell

DYNAMIC EFFECT OF LOAD ON RESPONSE

It was studied whether the type of impact can be deduced from its effect on the load and on the response with respect to a quasi-static interaction ($T_L > T_S$). The interaction occurring when $T_L \ll T_S$ or $T_L \approx T_S$ is characterised by a dynamic effect of the load on the response and by a change in the load due to the response. In general, this mutual interaction is quantified separately by dynamic amplification factors (DAF) and by the change in magnitude and duration of the load. These concepts are related to the same hydro-structural interaction but are introduced from a different perspective.

The DAF, defined as the ratio between the magnitude of the dynamic and the static structural response, is related to the question whether a static or a dynamic calculation is required for a given load, independently of the fact whether this load is measured on a rigid or flexible structure. The load change, on the other hand, is related to the question whether the load can be measured on a rigid structure, although it represents the load on a flexible structure. The term hydro-elasticity is sometimes used to refer to this load change. However, the term hydro-elasticity is used throughout this paper to refer to the hydro-structural interaction occurring when $T_L \ll T_S$ or $T_L \approx T_S$, and is therefore not limited to the load change.

A load change is expected for the crest load, because the interaction has found to be not quasi-static. The hydrodynamic mass component observed after the peak pressure, is an example of the expected load change. However, the question is if the peak pressure is also affected. The comparison between the pressures measured during full scale tests on the rigid structure and on the NO96, is biased because this local load is not two-dimensional. A static evaluation of the measured pressures on both structures is therefore required.

In this study, we focus on the effect of the load on the response. The probability of a load change equals the probability of a dynamic effect of the peak pressure. Advancements in numerical simulations as Guilcher et al. (2010), will help to quantify the extent of the load change by means of parametric studies. The long term goal is to define whether the load changes can be neglected despite the fact that dynamic effects of the load on the response occur.

The effect of the load on the response is studied by a comparison of a dynamic and a static response. The dynamic response is measured. The static response needs to be calculated for the measured load. A numerical or an experimental defined stiffness matrix can be used. Also here, the difficulty lies in the fact that local loads are not necessarily completely captured. Numerical simulations are used to investigate the consequences.

Global deformation modes

From the full scale tests, it is apparent that a load affects the structure beyond its loaded area. Global deformation modes are involved both for quasi-static and dynamic loads. The fact that a cell deflects upwards when the trough loads the cell underneath statically, indicates that modes, spatially more global than the bending of a cell, play a roll. Likewise, it was observed that global modes are excited by local loads.

As a consequence, when the strain is calculated with a load that is not completely captured, it will differ from the measured strain. Static simulations are performed to quantify this difference. The FE model of NO96 presented in Pillon et al. (2009) is used. The model was calibrated with static measurements and verified with experimental defined mode shapes. Good correlation with the first natural modes was found.

The upper cell is loaded first, see Figure 17. A two-dimensional unit pressure is statically applied. The strain is evaluated in the middle of the two upper cells, representing a strain gauge, indicated by □ in the figures. A pressure gauge is thought to be placed in the same location on the upper cell. The response is summarised in Table 1. Here the strain is expressed as a function of the maximum strain ϵ_1. Next the upper cell is loaded by a combination of the two-dimensional pressure and the local pressure. Different loaded areas are considered (Figure 18). The

local load is not measured by the pressure sensor. The response is a linear combination of the response due to (1) a two-dimensional unit pressure and (2) a local unit pressure. It is apparent that the strain calculated with a load that is not captured completely, i.e. ϵ_1, significantly differs from the measured strain. The actual influence of the local pressure on the measured strain will not only depend on the loaded area, the location and the magnitude of the pressure but also on its load duration.

Analysing the effect of the load on the response by a comparison of the measured and the calculated strain, is therefore biased when local loads are involved. As a workaround, the effect of the load on the response can be evaluated based on calculated dynamic and calculated static responses. However, it provides only insight in the dynamic effect of the measured load, and not in the effect of the actual load. Also in this analysis, both a numerically and an experimentally defined stiffness matrix can be used. In addition, a mass matrix should be defined. In this paper, the determination and the application of an experimentally defined stiffness matrix is discussed next.

FIGURE 17: Two-dimensional load on upper cell of NO96. Loads measured by pressure gauge.

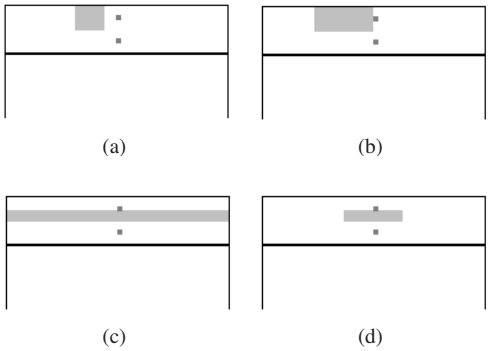

FIGURE 18: Local load on upper cell of NO96. Loads not measured by pressure gauge.

TABLE 1: Static response of NO96 cover plate for different loaded areas

Loaded area	Measured pressure	Measured strain on cell 1	Measured strain on cell 2
Figure 17	1	ϵ_1	$-0.15\epsilon_1$
Figure 17 + Figure 18a	1	$(1+0.11)\epsilon_1$	$-(0.15+0.01)\epsilon_1$
Figure 17 + Figure 18b	1	$(1+0.43)\epsilon_1$	$-(0.15+0.06)\epsilon_1$
Figure 17 + Figure 18c	1	$(1+0.42)\epsilon_1$	$-(0.15+0.04)\epsilon_1$
Figure 17 + Figure 18d	1	$(1+0.41)\epsilon_1$	$-(0.15+0.05)\epsilon_1$

Boundary conditions

An experimentally defined stiffness matrix is studied because staples, used for the assembly of the boxes, can introduce local structural behaviour that is normally not modeled in a FE model. The boundary conditions, i.e. the connection between the cover plate and the bulkheads are defined by the staples. The connection is often idealized as either clamped or hinged, even tough, it behaves most of the time in between. This can be modeled as a hinged connection combined with a rotational spring. In Pillon et al. (2009), a non-linear rotational spring was considered. The ratio between the rotational spring stiffness and the bending stiffness of the structure, defines the boundary condition. For a given rotational spring, the connection changes from hinged to clamped, i.e. from flexible to stiff, when decreasing the bending stiffness.

The boundary conditions significantly influence the structural response of the cover plate and the bulkheads. The bending of the cover plate is larger for a flexible connection compared to a stiff connection. On the other hand, a small moment is applied on the bulkheads in case of a flexible connection. As a consequence, the bulkheads bend slightly. When the connection is stiffener, a larger moment is transmitted by the loaded cover plate to the bulkheads. As a result, the bulkheads will bend more. This is illustrated in Figure 19. The dynamic properties of the assembly are also related to the boundary conditions. The first natural frequency of a clamped beam is twice the frequency of a hinged supported beam.

Evidence was found in Figure 6 that the staple connections are not identical within the box. The observations are in line with above presented theory: small deflections of the cover plate are accompanied by large deflection of the bulkhead. In addition, differences were observed in terms of the translational stiffness, in Figure 10. Taken together, an appropriate model of the connections is essential to evaluate the structural response. Peculiarities were observed that are normally not modeled in a FE model. The possibilities of an experimentally defined stiffness matrix are therefore explored.

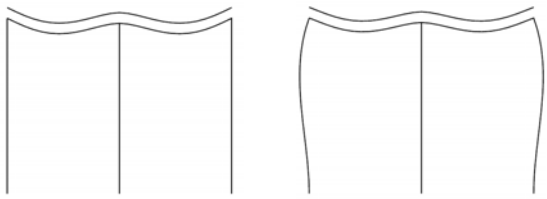

FIGURE 19: Flexible (a) and stiff (b) connection between cover plate and bulkhead - illustrated for a two bulkhead model.

Experimentally defined stiffness matrix

First, it is described how the stiffness matrix is defined and derived. Then, the matrix is applied for the slosh and the air pocket impact given in Figure 4 and 8 , respectively.

The stiffness matrix of a finite element is defined as the relation-

ship between the nodal forces and the nodal displacements. For a element with n degrees of freedom, the relation is given by:

$$\boldsymbol{F} = K\boldsymbol{v} \tag{1}$$

Here $\boldsymbol{F} = (F_1, F_2, \ldots, F_n)^t$, $\boldsymbol{v} = (v_1, v_2, \ldots, v_n)^t$ and are the nodal forces and the nodal displacements, respectively. K is a $n \times n$ stiffness matrix. Examples of basic finite elements are: a two node beam, a four node plate, an eight node solid, etc. These finite elements are combined to represent the structure and are described by a global stiffness matrix.

In this study, a new basic element is derived, i.e a n-node NO96 box element. Because, only one box is studied in the paper, the global stiffness matrix equals the matrix of the basic element. Each node has one degree of freedom. The pressure field on the element can be described as a function of the nodal forces:

$$p(\boldsymbol{x}) = \boldsymbol{N}_p(\boldsymbol{x})\boldsymbol{F} \tag{2}$$

$\boldsymbol{N}_p(\boldsymbol{x})$ is the shape function matrix for the pressure. It follows that the pressures at the nodes, $\boldsymbol{p} = (p_1, p_2, \ldots, p_n)^t$, are defined as:

$$\boldsymbol{p} = \mathcal{N}_p\boldsymbol{F} \tag{3}$$

whereby $\mathcal{N}_p = (\boldsymbol{N}_p(\boldsymbol{x_1}), \ldots, \boldsymbol{N}_p(\boldsymbol{x_n}))^t$. In this study, the pressure field consists of n loaded areas (A_i), each related to one node over which the pressure is constant:

$$F_i = \begin{cases} p_i A_i \text{ , } \boldsymbol{x} \in A_i \\ 0 \text{ , elsewhere} \end{cases} \tag{4}$$

The displacement field of the element can also be given as function of the nodal displacements

$$u(\boldsymbol{x}) = \boldsymbol{N}_u(\boldsymbol{x})\boldsymbol{v} \tag{5}$$

Differentiating the displacement field defines the strain field of the element. Each component of the strain tensor ϵ can be written in terms of a differential operator matrix $\boldsymbol{D}$:

$$\epsilon(\boldsymbol{x}) = \boldsymbol{D}(\boldsymbol{x})u(\boldsymbol{x}) \tag{6}$$

It follows that the strains at the nodes, $\boldsymbol{\epsilon} = (\epsilon_1, \epsilon_2, \ldots, \epsilon_n)^t$, are defined as:

$$\boldsymbol{\epsilon} = \mathcal{E}\boldsymbol{v} \tag{7}$$

whereby $\mathcal{E} = (\boldsymbol{D}(\boldsymbol{x_1})\boldsymbol{N}_u(\boldsymbol{x_1}), \ldots, \boldsymbol{D}(\boldsymbol{x_n})\boldsymbol{N}_u(\boldsymbol{x_n}))^t$. The relation between the pressure and strain at the nodes of the n-node NO96 box element is:

$$\boldsymbol{p} = \mathcal{K}\boldsymbol{\epsilon} \tag{8}$$

with

$$\mathcal{K} = \mathcal{N}_p K \mathcal{E}^{-1} \tag{9}$$

The matrix $\mathcal{K}$ is experimentally determined by regression modeling based on observations for each p_i and ϵ_i. The r-th observation of p_i is given as a function of the unknowns k_{ij} by

$$p_i^r = \boldsymbol{e^{r,i}} \cdot \boldsymbol{k} \tag{10}$$

whereby $\boldsymbol{k} = (k_{11} \cdots k_{1n}, \ldots, k_{n1} \cdots k_{nn})^t$ and $\boldsymbol{e^{r,i}} = (e_1^{r,i}, e_2^{r,i}, \ldots, e_{n^2}^{r,i})^t$ with

$$e_l^{r,i} = \begin{cases} (\epsilon_1^r, \epsilon_2^r, \ldots, \epsilon_n^r) \text{ , } l = (i-1)n+1 : (i-1)n+n \\ 0 \text{ , elsewhere} \end{cases} \tag{11}$$

When $m \times n > n^2$, we have an overdetermined system in function of the unknowns k_{ij}

$$\tilde{\boldsymbol{p}} = E\boldsymbol{k} \tag{12}$$

with $\tilde{\boldsymbol{p}} = (p_1^1 \cdots p_n^1, \ldots, p_1^m \cdots p_n^m)^t$ and $E = (\boldsymbol{e}^{1,1} \cdots \boldsymbol{e}^{1,n}, \ldots, \boldsymbol{e}^{m,1} \cdots \boldsymbol{e}^{m,n})^t$.

A symmetric stiffness matrix ($k_{ij} = k_{ji}$) is assumed as it limits the required number of independent observations. The problem reduces to $(n^2 - n)/2 + n$.

The stiffness matrix is based on impact tests whereby the hydro-structural interaction is quasi-static. The trough load during a slosh impact and the air pocket loading were found to be quasi-static. Only one independent observation can be made over the width of the box, because the load is two-dimensional in case of the trough and the air pocket load. Eight pressure sensors were placed over the height of the box. Taken together, a maximum of eight degrees of freedom can be studied with 36 unknown k_{ij} for a symmetric matrix.

In contrast to the air pocket load, the trough load allows us to define independent observations of $\boldsymbol{p}$, because the trough loads the cells successively. First, only the lower cell is loaded, then the lower two, etc. One slosh is sufficient to define the 36 unknown k_{ij} with Eq. 12. The measured pressures and strain at the middle vertical line on the box are used.

The experimentally defined stiffness matrix is applied to the slosh impacts given in Figure 4. The measured strains $\boldsymbol{\epsilon}$ are multiplied with $\mathcal{K}$, and compared to the measured pressures in Figure 20. The measured and the calculated pressure represent the static and the dynamic response, respectively. When a quasi-static load is applied, the dynamic response equals the static response. The calculated pressure should therefore be equal to the measured pressure, when a quasi-static load is applied. Owing to the fact that the measured and the calculated pressure are equal in Figure 20, it can be concluded that the experimental stiffness matrix is well defined for the trough load. In addition, it is demonstrated that it is insufficient to consider only the diagonal elements of the stiffness matrix. The effect of the global deformation modes can not be neglected.

$\mathcal{K}$ is also applied to the air pocket impacts given in Figure 8. It is apparent that for the quasi-static air pocket load, the matrix is only well defined during the compression. It has been demonstrated in this study that different deformation modes are involved during the compression and the expansion of the air pocket. The structure response is non-linear and is therefore not well described by a linear description of the stiffness matrix. $\mathcal{K}$ will be representative when similar deformation modes are

involved as during the trough load.

The interaction was not quasi-static for the crest load. Differences between the measured and the calculated pressure are therefore expected. The differences are a function of the mass matrix. Difference are observed in case Figure 21b. An amplification seems to be present ($T_L \approx T_S$). However, the difficulty here is to evaluate whether these differences are (1) due to the dynamic effect of the load or (2) due to uncertainties in the stiffness matrix. As concluded before, more pressure gauges are required to capture the crest load and thus more degrees of freedom are required in the n-node NO96 element.

In general, therefore, the advantage of an experimentally defined NO96 element is that it considers the actual boundary connections. The disadvantage is that it is limited to one degree of freedom over the width of the box. The local loads which are three-dimensional in nature, and their global structural response are therefore not well enough described. It will be investigated whether a numerically defined n-node NO96 element - with n the number of pressure sensors - can be combined with the experimentally defined one.

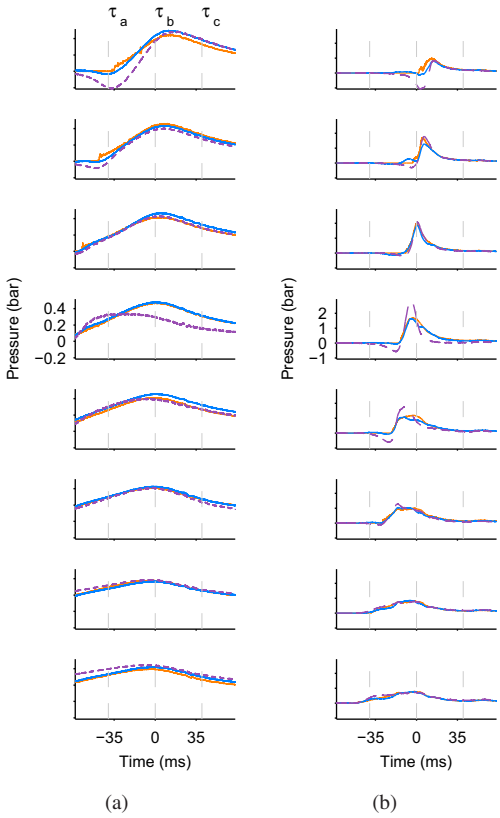

FIGURE 20: Measured pressures (—) compared to pressures calculated with measured strain and stiffness matrix (—) and compared to pressures calculated with measured strain and diagonal elements of stiffness matrix (- -). Slosh impacts of Figure 4

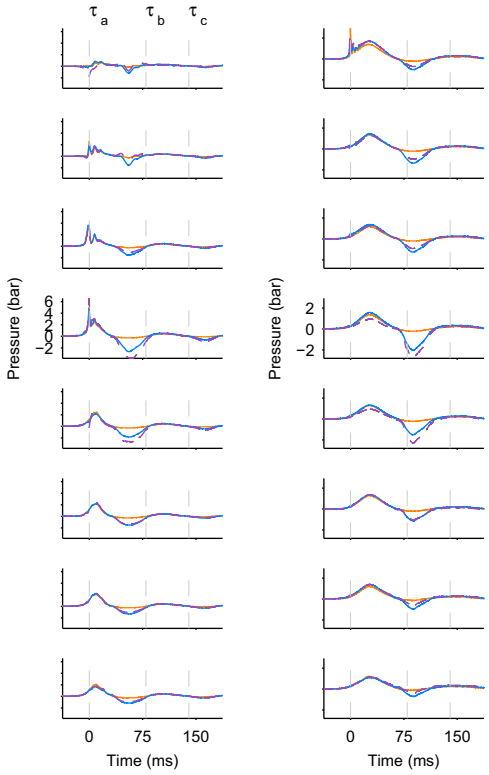

FIGURE 21: Measured pressures (—) compared to pressures calculated with measured strain and stiffness matrix (—) and compared to pressures calculated with measured strain and diagonal elements of stiffness matrix (- -). Air pocket impacts of Figure 8.

CONCLUSIONS

This paper has presented the behaviour of the NO96 membrane containment system when subjected to breaking wave impacts. The data obtained from the full scale impact tests in the Sloshel project, have significantly enhanced the understanding of the hydro-structural interactions that occur between the breaking wave and the NO96.

The following main conclusions can be drawn from the present study: (1) local loads are not necessarily filtered by the structure, just because they are related to small loaded areas and short load durations, (2) local loads affect the structure beyond their loaded area, and (3) local loads will only be captured partially by a discrete set of pressure gauges. The question, however, whether it is essential that all local loads are captured, should be answered in relation to the strength of the structure. The higher the pressures are, the smaller the loaded area and the shorter the durations will be. Because material properties are related to these load durations, the pressure should at least be captured over an area that is effective in terms of the strength.

The long term goal is to validate todays engineering approach to include the dynamic effect of the load on the structural response

and to define whether the accompanying load changes can be neglected. Parametric FE simulations with simplified pressure fields will be carried out next to investigate further the hydro-structural interactions that can occur when local loads are involved. It has been observed in this paper that the loading on the whole NO96 - even tough it is partially quasi-static - should be considered in these simulations. Moreover, the application of a numerically n-node NO96 element - with n the number of pressure sensors - combined with an experimental one, will be studied.

REFERENCES

Bogaert, H. and Kaminski, M. (2010). Advances in sloshing assessment from the Sloshel project, *Proceedings of 20th International Offshore and Polar Engineering Conference, June 20-26, Bejing, China*.

Bogaert, H., Leonard, S., Kaminski, M. and Brosset, L. (2010). Sloshing and scaling: results from Sloshel project, *Proceedings of 20th International Offshore and Polar Engineering Conference, June 20-26, Bejing, China*.

Guilcher, P.-M., Oger, G., Brosset, L., Jacquin, E., Grenier, N. and Touze, D. L. (2010). Simulation of liquid impacts with a two-phase parallel SPH model, *Proceedings of 20th International Offshore and Polar Engineering Conference, June 20-26, Bejing, China*.

Kaminski, M. and Bogaert, H. (2010). Full-Scale Sloshing Impact Tests Part I, *International Journal of Offshore and Polar Engineering* **20**: 1–10.

Pillon, B., Marhem, M., Leclère, G. and Canler, G. (2009). Numerical Approach For Structural Assessment of LNG Containment Systems, *Proceedings of 19th International Offshore and Polar Engineering Conference, June 21-26, Osaka, Japan*.

ACKNOWLEDGEMENTS

The views expressed in the paper are those of the authors and do not necessarily represent the unanimous views of all the consortium members.

The authors would like to acknowledge the support provided by the Sloshel consortium members that have made the Sloshel project possible: American Bureau of Shipping, Bureau Veritas, Ecole Centrale Marseille, Chevron, ClassNK, Det Norske Veritas, GTT, Lloyd's Register, MARIN and Shell. The support provided by the subcontractor Deltares is appreciated.